Global Identification of a Low-Order Lumped-Parameter Thermal Network for Permanent Magnet Synchronous Motors

Article *in* IEEE Transactions on Energy Conversion · September 2015

DOI: 10.1109/TEC.2015.2473673

CITATIONS
145

READS
2,270

2 authors:

Oliver Wallscheid
Universität Paderborn
127 PUBLICATIONS **1,558** CITATIONS

SEE PROFILE

Joachim Böcker
Universität Paderborn
308 PUBLICATIONS **3,660** CITATIONS

SEE PROFILE

Global Identification of a Low-Order Lumped-Parameter Thermal Network for Permanent Magnet Synchronous Motors

Oliver Wallscheid, *Student Member, IEEE,* Joachim Böcker, *Senior Member, IEEE*

***Abstract*—Monitoring critical temperatures in permanent magnet synchronous motors (PMSM) is essential to prevent device failures or excessive motor life time reduction due to thermal stress. A lumped-parameter thermal network (LPTN) consisting of four nodes is designed to model the most important motor parts, i.e. the stator yoke, stator winding, stator teeth and the permanent magnets. An empirical approach based on comprehensive experimental training data and a particle swarm optimisation are used to identify the LPTN parameters of a 60 kW automotive traction PMSM. Varying parameters and physically motivated constraints are taken into account to extend the model scope beyond the training data domain. Here, a so-called global identification technique for linear parameter-varying (LPV) systems is innovatively applied to a thermal motor model for the first time. The model accuracy is cross-validated with independent load profiles and a maximum estimation error (worst-case) of 8 °C regarding all considered motor temperatures is achieved. Also, a comprehensive residual statistical analysis proves suitable estimation results in terms of model robustness and accuracy.**

***Keywords*—Permanent magnet machines, temperature sensors, thermal analysis, temperature dependence, thermal management, estimation, system identification, particle swarm optimisation**

I. Introduction

The permanent magnet synchronous motor (PMSM) is used in many industrial applications nowadays. Due to the improvement of permanent magnet (PM) materials over the last decade, the PMSM became leading in terms of torque and power density with respect to volume and weight. In automotive applications these characteristics are crucial and thus the PMSM is favourably chosen in comparison to other motor types. From a device utilisation point of view the component temperature in the different motor parts is one of the most essential aspects to consider. While excessive magnet temperatures involve the risk of irreversible demagnetisation, exceeding the thermal limits of the winding can destroy the insulation varnish. Besides the prevention of partial or total motor destruction, intensive thermal stress can lead to a shortened device life time [1], [2]. Real-time temperature estimation of critical motor components can be used as the input quantities of derating controllers [3]. Hence, safe motor operations can be guaranteed while maximising the thermal device utilisation during runtime and reducing material employment in the motor design phase to a minimum. In this context, the use of cost-intensive dysprosium to increase the temperature stability of neodymium-iron-boron (NdFeB) magnets should be mentioned [4], [5]. Moreover, the influence of temperature-dependent electrical parameters on the motor control performance (e.g. torque accuracy due to PM flux linkage variation) can be compensated, if real-time temperature information is available [6], [7].

Today, the measurement of the winding or end-winding temperature with standard thermal sensors is state-of-the-art in many industrial applications. However, since these sensors are usually difficult to access, they cannot be simply replaced in case of failures. Also, sensor detuning effects can occur within the device lifespan and should be detected with respect to functional safety issues. Therefore, redundant temperature information is required. Additionally, direct measurement of the PM temperature is a challenging task. Here, techniques like infrared thermography (limited to surface magnets) as well as standard thermal sensors combined with wireless or slip-ring signal transmission [8]–[10] have to be applied. However, these methods are not suitable for medium and large scale industrial production due to their additional costs and constructional drawbacks.

Against this background, model-based approaches to indirectly obtain the component temperatures under real-time requirements were investigated in the last years. Approaches to estimate the PM temperature are based on electrical machine models, either by utilising a precise flux observer [11] or signal injection methods [12], [13]. Also, to retrieve the winding temperature observer as well as signal injection methods are available [14]. In both cases, temperatures are determined indirectly by utilising the thermal properties of electric model parameters, e.g. the winding resistance or the PM flux linkage. However, commonly employed PM materials (e.g. NdFeB) show only a low temperature sensitivity and the ohmic voltage drop in high-power machines is only small in contrast to the total terminal voltage [14]. Accurate temperature estimations therefore always require comprehensive modelling efforts, i.e. motor and inverter parameters have to be precisely identified. Consequently, parameter discrepancy can lead to enormous temperature estimation errors [15]. In addition, signal injection leads to additional losses and may not be suitable for some applications due to electromagnetic interference issues. A suitable alternative to determine critical component temperatures are lumped parameter thermal networks (LPTN). These are based on the idea to simplify the complex thermal behaviour of a given system and to abstract the heat transfer processes by using equivalent circuit diagrams. The major analogies between LPTN and electrical circuits are summarised in [16], [17].

In this contribution a 60 kW automotive traction PMSM prototype is investigated. This motor type is built with a concentrated winding scheme and interior magnets. As a special and very important boundary condition it should be noted that several material and geometric motor information are missing (not provided by manufacturer):

- The totally enclosed water cooling jacket construction (i.e. channel shape) is unknown
- Details about the winding configuration (i.e. wire shape and insulation thickness, filling factor, etc.) are missing
- An electromagnetic finite-element-analysis (FEA) model is also not available (i.e. unknown loss distribution inside the motor)

However, the motor's cross section (see Fig. 1) and other basic material information (e.g. PM-material details, steel sheet data, etc.) are known. Thus, one major objective of this contribution is to deal with uncertainty regarding the thermal modelling process while incorporating the available system knowledge. Hence, an empirical approach utilising experimentally gained test bench data is applied to identify the LPTN parameters by means of particle swarm optimisation and a-priori knowledge of the general system behaviour. Here, another focus lies on suitable identification methods for linear parameter-varying (LPV) systems since many LPTN parameters regarding electrical drives are not constant in the entire operation range.

II. State-of-the-Art

Typically thermal analyses can be carried out using computational fluid dynamics (CFD), heat equation finite element analysis (FEA) or LPTN models [18]. The first two are very accurate and deliver proper predictions of the thermal system behaviour

O. Wallscheid and J. Böcker are with the Department of Power Electronics and Electrical Drives, University of Paderborn, 33098 Paderborn, Germany, e-mail: {wallscheid, boecker}@lea.uni-paderborn.de

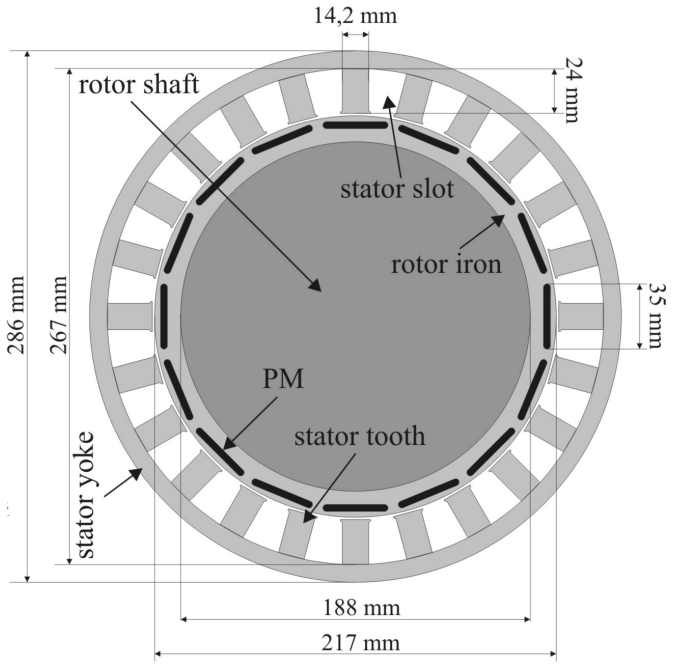

Fig. 1. Cross section of investigated PMSM with interior magnets and concentrated winding ($P_n = 60$ kW, axial iron length $l = 95$ mm)

during the device development. However, the heat equation FEA approaches are very limited regarding the modelling of convection processes, which is indeed fairly important in the electric motor context (due to air-gap and end-cap turbulences, rotating rotor shaft, etc.). Consequently, CFD methods are considered as most accurate for thermal motor modelling [18]. Nevertheless, both methods require enormous computational resources making them unsuitable for any real-time monitoring nowadays and in the medium run. Thus, less computationally demanding LPTN approaches will be discussed more detailed.

A. Lumped-Parameter Thermal Networks

In general, one can find three different ways for designing a LPTN with respect to electric motor applications:

- *Dark grey-box LPTN*: Here, thermal networks of lowest order (2-5 nodes) are used to model the most dominant heat paths. These LPTNs are strongly abstracted and can be designed with minor physical knowledge regarding the modelling of heat exchange processes in complex thermal structures. Hence, thermal parameters are mostly identified based on experimental training data [17], [19]–[22].
- *Light grey-box LPTN*: The important motor components are analytically modelled at rather low local discretisation levels based on heat transfer theory. Typical model orders are in the range of 5-15 nodes. The model parameters are calculated based on material and geometrical data, but can be optimised with respect to empirical measurements [16], [23]–[28].
- *White-box LPTN*: These are modelled based on heat transfer theory relying solely on material and geometrical motor data. However, as compared to light grey-box LPTN, certain critical or important motor parts, such as the end-windings, are modelled at very high local discretisation levels, i.e. they are divided into fine meshes with respect to Cartesian or cylindrical coordinates leading to a remarkable number of nodes [29]–[33].

As LPTN inherently specify a certain model structure in accordance with the basic formulations of heat transfer theory, they cannot be classified as black boxes. Instead, approaches like recurrent neutral networks can be investigated as thermal black box models for electrical traction drives [34].

White-box LPTN allow an accurate modelling and the opportunity to estimate the hot-spot temperatures inside the different motor components (e.g. winding). As shown in [35] a relatively high number of nodes per motor component is required to enable a proper distinction between the average and the hot-spot temperature. Therefore, white-box LPTN are successfully applied in the motor development phase to predict the thermal motor behaviour of new motor designs for many years [18]. In direct comparison to FEA and CFD approaches the required computational resources are reduced and thus motor design optimisations can be carried out faster [36]. However, white-box approaches based on the classical T-equivalent-circuit-method [25] or the k-shift-approach [32] still lead to large differential-algebraic-equation (DAE) systems. Thus, real-time execution of white-box LPTN is not feasible for many cost-sensitive applications with very limited digital processing units. As an example automotive applications can be mentioned since the pricing pressure is very high in this industry and the typically applied (cheap and inefficient) electronic control unit (ECU) has to handle multiple task (e.g. main drive control, functional safety monitoring, etc.). It is also obvious that full material and geometric information have to be available, which may not always be the case (e.g. older prototype motors).

Grey-box LPTN are distinctly more abstract as the motor components are not divided into several sub-nodes. Therefore, grey-box LPTN are always estimating the component average temperature and consequently lacking important hot-spot information [35]. As shown in [19] this problem can be overcome by using empirically obtained data regarding the relationship between average and hot-spot temperature of a given motor component. Otherwise, more conservative safety margins regarding the temperature limits during operation should be chosen if only the average temperatures are estimated. The main advantage of this LPTN class is the small node amount and the reduced computational demand making it suitable for real-time temperature monitoring in many applications. In the last years many different grey-box LPTN approaches have been proposed mainly differing in their node amount (i.e. how many different motor components are considered) and in their way of derivation (i.e. analytical or empirical identification focus).

B. Identification of linear parameter-varying systems

Accurate thermal modelling in terms of LPTN approaches requires to take varying parameters into account, e.g. varying thermal resistance between rotor and stator components due to speed-dependent air gap convection [37]. In this exemplary case the motor speed is the so-called scheduling variable which influences the model parameter (thermal resistance value). Consequently, LPTN are linear parameter-varying (LPV) models making parameter identification more complex in comparison to well-known linear time-invariant (LTI) systems. In general, LPV parameter identification can be realised in two different ways [38], [39]: Following the *local approach* several independent experiments are carried out in the complete scheduling plane (operation area of the scheduling variables). Here, the scheduling variables are kept constant in each single experiment and only the model inputs are excited. Thus, a LTI model can be identified for each local experiment and afterwards all LTI models are merged together to one LPV model. The advantage of the local approach is the good estimation accuracy around the considered scheduling variable operating points, but merging together all independent LTI models can lead to inconsistent and non-robust LPV models [40]. This is a very critical issue for LPTN-LPV-identification as the thermal system response to a given excitation (motor losses) cannot be completely recorded in the overload operation range (thermal limits are reached before steady-state). Thus, the local LPV-identification of LPTN inherently lacks the overload operation range and the identified LPTN is only valid for

continuous power operations. This is a severe drawback for many applications with dynamic load profiles (e.g. traction drives) as the estimated temperature information is highly uncertain during the overload phases. However, in the field of thermal motor modelling [17], [19], [20], [22] and also other engineering applications [38], [41], [42] the local approach is clearly dominating in the existing literature. It is also very interesting to note that most publications dealing with experimental identified LPTN don't address the above mentioned overload issue.

In contrast, the scheduling variables and the model inputs are simultaneously and persistently excited in the *global approach*. The LPV model parameters are directly identified by utilising empirical data of one comprehensive experiment leading to more robust results. Therefore, more a-priori system knowledge has to be incorporated to reduce the possible search room of the unknown parameter set. Hence, the general relationship between the considered varying parameters and their scheduling-variables has to be predefined by the model designer as a framework for the global LPV identification. In the LPTN case, a broad and well-established knowledge base regarding the general thermal processes is available in the literature (i.e. basic analytical formulation from [23], [25] or many other). Consequently, the motor overload operation range can be incorporated within the experimental training data as a complete decay of thermal transients is not required. Despite this essential advantage of global towards local LPV-identification approaches, global approaches are absolutely rare in the existing literature. Only in purely academic and artificial studies [43], [44] and in the context of a simplified transformer LPTN with simple load profiles (especially without overload operation) [45] global LPV identifications can be found. Complex LPV systems (e.g. motor LPTN) were not globally identified, yet.

III. Proposed Framework for Global LPV-LPTN-Identification

The focus of this contribution is to prove the feasibility of global LPV identification to LPTN addressing the complex thermal behaviour of PMSM as an extension of the literature state-of-the-art. Besides that, the proposed identification methods is designed to handle serious information uncertainty regarding important motor material and geometric information. Against the background, a general modelling framework incorporating low to medium a-priori system knowledge is proposed. Thus, the presented approach can be classified somewhere in between the dark- and light-grey box LPTN models.

In Fig. 2 the LPTN structure utilised to model the thermal behaviour of the investigated PMSM is shown. This design is quite abstract as only the most dominant heat paths are considered. Therefore, the modelling depth is rather low, but the implementation and calculation effort are very computationally efficient. The LPTN consists of four nodes representing the stator yoke temperature ϑ_{SY}, the stator teeth temperature ϑ_{ST}, the stator winding temperature ϑ_{SW} and the permanent magnet temperature ϑ_{PM}, respectively. Each node is connected to the thermal ground potential via a thermal capacitiy C to represent the thermal system dynamics. The cooling liquid temperature ϑ_C and the ambient air temperature ϑ_A are assumed to be measured quantities and therefore depicted as temperature sources. The thermal resistance $R_{i,j}$ model the heat flow from node i to node j. Moreover, the losses P_v in the different motor components are introduced as heat sources representing the inner heat generation within the system. To describe the thermal motor behaviour the following assumptions are made [25]:

- Each considered motor component has a homogeneous temperature distribution
- Due to the concentrated winding scheme the end-winding temperature equals the slot temperature
- The heat generation and thermal capacity are uniformly distributed
- The permanent magnet temperature is representative for the complete rotor
- The dominant heat paths are considered in the LPTN (Fig. 2), other heat paths can be neglected

The second assumption regarding the end-winding temperature is based on experimental experience with the investigated PMSM prototype. This assumption should not claim universal validity for all PMSM with concentrated winding scheme (and certainly not for distributed winding motors), but is applicable for this given motor. In Fig. 3 the winding and end-winding temperature is compared for the load profile given in Fig. 7 to prove the assumption within this contribution. Nevertheless, the proposed LPTN design depicted in Fig. 2 as well as the following general model framework and identification process can be easily extended to include an end-winding node.

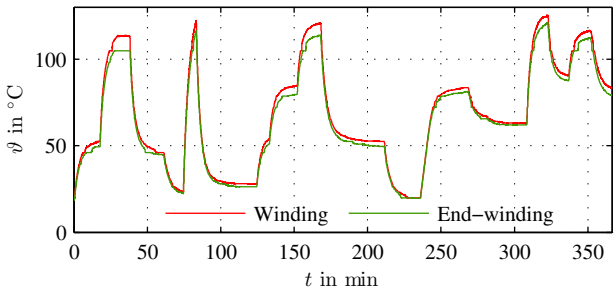

Fig. 3. Experimental measurement of winding and end-winding stator temperature for load profile shown in Fig. 7

A. Loss Model and Test Bench Design

The motor losses are of major interest as they describe the inner heat generation within the thermal motor system. Thus, it is desirable to get detailed insights into the motor loss characteristics and its local distribution. Typically, electromagnetic finite element analysis (FEA) is carried out to get this information, however, an electromagnetic FE model of the investigated PMSM is not available. Notwithstanding the above, it should be noted that loss calculation via FEA for traction applications requires significant efforts as the current control behaviour and the switching inverter characteristics have to be taken into account [46]. Otherwise, serious deviations between FEA simulation and the actual motor loss characteristics can occur.

To overcome the missing electromagnetic FE model a more empirical loss modelling approach has to be realised. Therefore, the overall motor losses were measured in the entire speed-torque-plane $P_v(n,T)$ at an automated automotive test bench inside the department's laboratory. For simplification reasons only positive speed values had been considered, but the following approach can be easily extended to the negative speed plane, as well. An accurate Yokogawa WT3000 power meter combined with Danfysik Ultrastab 867-700I current transducers and a HBM T10F torque transducer were used. The motor speed was kept constant with a suitable load machine and the investigated PMSM was fed by a standard 2-level-B6-inverter from Semikron. The motor control and measurement signal recording was realised with a dSPACE DS1006 processor board. Also, the measurement automation was realised on the processor board. A standard field-oriented control structure with superimposed open-loop torque control strategy was used (see [47], [48] for details). During power loss measurements all motor component temperatures had been kept constant to exclude influences from temperature-dependent loss changes within the recorded data.

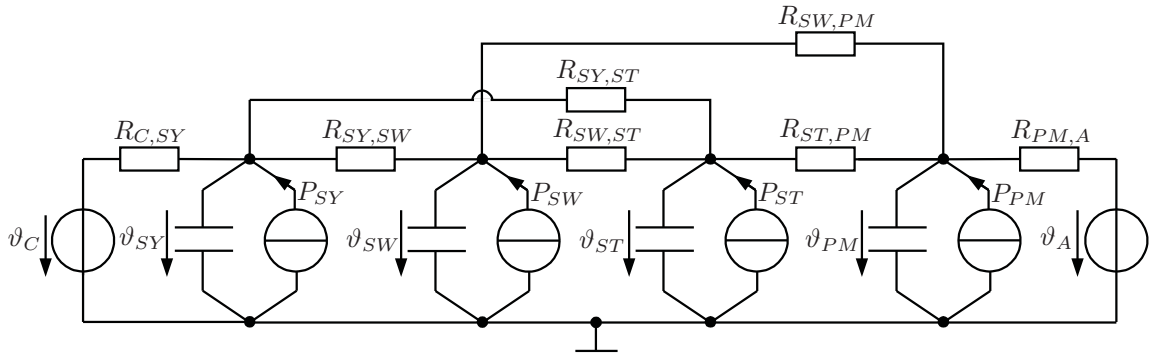

Fig. 2. Structure of the proposed lumped parameter thermal network (LPTN)

Therefore, the PMSM is equipped with 16 thermocouples distributed inside the stator and 8 inside the rotor (all of type K, class 1). The rotor thermocouples are distributed closely around different PM elements to measure a representative PM average temperature. The PM temperature signals were transferred by a commercial telemetry system from the rotor part to the DS1006 controller board. More information regarding the test bench configuration can be found in [49].

The measured power losses $P_v(n,T)$ had been converted to the speed-current-plane since the relationship between motor torque and stator current can change significantly when operating in the flux weakening mode. This can be explained due to the temperature-dependent change of the permanent magnet flux linkage in combination with a superimposed voltage controller in the flux-oriented control scheme of traction drives [50]. The measured losses are depicted in Fig. 4. Here, I is the RMS-current, i_q is the q-part of the stator current in flux-oriented coordinates and n is the motor speed. The i_q-sign has to be taken into account since the loss characteristics slightly differ in motoring and generating operations. In addition, it is assumed that mechanic losses (friction) can be neglected. The data $P_v(I\cdot\mathrm{sign}(i_q),n)$ can be saved as a look-up table (LUT) in the drive control memory guaranteeing accurate loss information during runtime. It should also be mentioned that the measurements are only valid for one given DC-link voltage due to the switching of the feeding inverter. Hence, Fig. 4 has to be identified at different DC-link voltages for certain applications (e.g. battery electric vehicles). In this contribution a varying DC-link voltage is neglected for the sake of clarity.

The copper losses can be calculated during runtime based on the actual current. It is assumed that the copper losses are equal to the stator winding losses:

$$\begin{aligned} P_{v,Cu} &= P_{v,SW} = 3\cdot I^2\cdot R_s(\vartheta_{SW},n)\\ R_s(\vartheta_{SW},n) &= R_{s,0}\cdot f_1(\vartheta_{SW})\cdot f_2(n)\\ f_1(\vartheta_{SW}) &= 1+\alpha_{Cu}\cdot(\vartheta_{SW}-\vartheta_{SW,0})\\ f_2(n) &= 1+\beta_{Cu,1}\cdot(n/n_{max})+\beta_{Cu,2}\cdot(n/n_{max})^2 \end{aligned} \tag{1}$$

Here, R_s is the ohmic resistance, f_1 models the copper resistance temperature-dependence and f_2 describes the skin- and proximity-effect influences. In (1) only $\alpha_{Cu}=0.39\,\%/\mathrm{K}$ and $R_{s,0}$, the reference resistance at standstill, are known a-priori. The coefficients $\beta_{n,1}$ and $\beta_{n,2}$ will be estimated within the parameter identification process. The resulting difference between the copper losses $P_{v,SW}$ and the overall losses P_v are called residual losses and assumed to equal the iron losses in the stator and rotor parts:

$$\widetilde{P}_{v,res} = \widetilde{P}_{v,Fe} = P_v(I,i_q,n) - \widetilde{P}_{v,SW}(I,n,\vartheta_{SW,0}) \tag{2}$$

Here, $\widetilde{P}_{v,SW}$ denotes the equivalent copper losses at reference temperature $\vartheta_{SW,0}$. The reference temperature is defined during the loss measurement, since the data from Fig. 4 is only valid

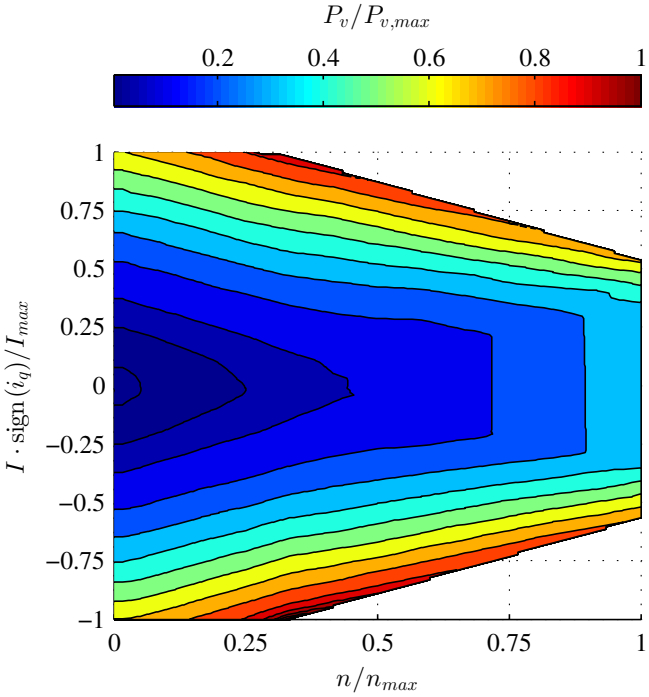

Fig. 4. Normalised electric losses in the speed-current-plane measured at constant motor temperatures

at a given temperature set. Then, the residual losses at reference temperature have to be assigned to the three other nodes:

$$\begin{aligned} \widetilde{P}_{v,s} &= k_1(I,n)\cdot\widetilde{P}_{v,res}\\ \widetilde{P}_{v,r} &= \widetilde{P}_{v,PM} = [1-k_1(I,n)]\cdot\widetilde{P}_{v,res}\\ \widetilde{P}_{v,SY} &= k_2(I,n)\cdot\widetilde{P}_{v,s}\\ \widetilde{P}_{v,ST} &= [1-k_2(I,n)]\cdot\widetilde{P}_{v,s} \end{aligned} \tag{3}$$

First, $\widetilde{P}_{v,res}$ is split up into a stator $\widetilde{P}_{v,s}$ and rotor $\widetilde{P}_{v,r}$ portion via $k_1(I,n)$. This function is assumed to be a bivariate first-order polynomial depending on the motor speed and current:

$$\begin{aligned} k_1(I,n) &= k_{1,0}+k_{1,1}\cdot I+k_{1,2}\cdot n+k_{1,3}\cdot I\cdot n\\ \text{with}\quad k_1 &\in\{\mathbb{R}|0\le k_1\le 1\} \end{aligned} \tag{4}$$

This assumption is made since the iron losses depend on the current amplitude and harmonics (i.e. flux density distribution) as well as on the actual frequency. The coefficients are unknown and will be estimated within the parameter identification. Then, the stator losses are divided into the yoke and teeth portion via $k_2(I,n)$, which has the same form like (4):

$$\begin{aligned} k_2(I,n) &= k_{2,0}+k_{2,1}\cdot I+k_{2,2}\cdot n+k_{2,3}\cdot I\cdot n\\ \text{with}\quad k_2 &\in\{\mathbb{R}|0\le k_2\le 1\} \end{aligned} \tag{5}$$

It should be noted that with the above definitions of k_1 and k_2 it is always guaranteed to preserve the power balance:

$$\widetilde{P}_{v,res} = \widetilde{P}_{v,PM} + \widetilde{P}_{v,SY} + \widetilde{P}_{v,ST} \tag{6}$$

This is particular important to identify the LPTN parameter set in a robust and physically-meaningful way.

As the hysteresis and eddy current losses are also temperature-dependent, the iron losses at reference temperature are scaled to the actual component temperatures [51]:

$$\begin{aligned} P_{v,PM} &= \widetilde{P}_{v,PM} \cdot [1 + \alpha_{Fe} \cdot (\vartheta_{PM} - \vartheta_{PM,0})] \\ P_{v,SY} &= \widetilde{P}_{v,SY} \cdot [1 + \alpha_{Fe} \cdot (\vartheta_{SY} - \vartheta_{SY,0})] \\ P_{v,ST} &= \widetilde{P}_{v,ST} \cdot [1 + \alpha_{Fe} \cdot (\vartheta_{ST} - \vartheta_{ST,0})] \\ \text{with} \quad & \alpha_{Fe} \in \{\mathbb{R} | -1\ \%/\mathrm{K} \leq \alpha_{Fe} \leq 0\} \end{aligned} \tag{7}$$

As the iron losses decrease with rising temperature (especially the eddy current part) the temperature coefficient α_{Fe} is negative. The exact value of α_{Fe} depends on the iron steel sheet material, the permanent magnet material and also on the motor design [52]. Thus, it cannot be calculated a-priori and has to be estimated during the parameter identification.

B. Thermal Resistances and Capacities

The thermal capacity C_i of each node is given by the specific heat capacity c_i and component mass m_i:

$$C_i = m_i \cdot c_i \tag{8}$$

Although the cross-section and length of the motor are known (Fig. 1) some other uncertainties make it difficult to calculate C_i precisely for each node. For instance, the unknown stator slot composition (wire cross-section, insulation thickness and epoxy configuration, etc.) or uncertainty due to the abstract modelling of the rotor side with only one node can be mentioned [53]. Thus, all thermal capacities are also estimated in the identification process, although (8) is used to roughly calculate every C_i limiting the search room and consequently improving the identification process.

The proposed LPTN structure contains 7 thermal resistances. It is assumed that $R_{SY,SW}$, $R_{SW,ST}$ and $R_{SY,ST}$ are constants as they describe the heat transfer due to conduction inside the stator nodes. They can be approximated by

$$R_{i,j} = \frac{l_{i,j}}{\lambda_{i,j} \cdot A_{i,j}} \tag{9}$$

with l as the effective conduction length, A as the effective cross-section area and λ as the thermal conductivity [23]. The approximation (9) is utilised to limit the search room and $R_{SY,SW}$, $R_{SW,ST}$ as well as $R_{SY,ST}$ are also finally identified during the identification process.

The thermal resistance $R_{C,SY}$ describes the heat flow from the stator yoke to the water cooling jacket. Here, $R_{C,SY}$ is characterised by conduction as the heat flow passes the yoke steel sheets and the housing connection as well as by convection since the heat is dissipated at the cooling jacket surface. Due to the lack of detailed information regarding the channel shape $R_{C,SY}$ can only be calculated very roughly by the formulations in [54]. Hence, it has to be estimated during the identification process and the following assumption is made:

$$\begin{aligned} R_{C,SY} &= R_{C,SY,0} \cdot [1 + \alpha_{C,SY} \cdot (\vartheta_C - \vartheta_{C,0})] \\ \alpha_{C,SY} &\in \{\mathbb{R} | -1\ \%/\mathrm{K} \leq \alpha_{C,SY} \leq 0\} \end{aligned} \tag{10}$$

A constant and linear varying part depending on the actual cooling liquid temperature is necessary to consider the conduction part on the one hand and the convection influence on the other. Here, the temperature-dependent kinematic viscosity ν of the water will influence the Reynolds number characterising the convection into the liquid. As ν decreases with increasing liquid temperature, $\alpha_{C,SY}$ will be negative. Furthermore, the liquid flow rate is held constant during all experiments and its influence on $R_{C,SY}$ is neglected for this contribution.

The resistances $R_{SW,PM}$, $R_{ST,PM}$ and $R_{PM,A}$ are assumed to model heat transfer mainly based on convection. The first two describe the heat flow through the air gap between rotor and stator and the last one represents the abstract heat exchange between the rotor shaft and the ambient air around the test bench. The resistance $R_{PM,A}$ is called abstract since other heat paths, e.g. through the bearings or the thermal connection to the load machine via the rotor shaft, are only indirectly taken into account. Based on the analytical formulations in [37], [54] a simplified function for $R_{SW,PM}(n)$, $R_{ST,PM}(n)$ and $R_{PM,A}(n)$ depending on the motor speed is derived:

$$\begin{aligned} R_{i,j}(n) &= R_{i,j,0} \cdot e^{-\frac{n}{n_{max}} \frac{1}{b_{i,j}}} + a_{i,j} \\ R_{i,j,0} &\in \{\mathbb{R} | 0 \leq R_{i,j,0} \leq R_{i,j,0,max}\} \\ a_{i,j} &\in \{\mathbb{R} | 0 < a_{i,j} \leq a_{i,j,max}\} \\ b_{i,j} &\in \{\mathbb{R} | 0 \leq b_{i,j} \leq b_{i,j,max}\} \end{aligned} \tag{11}$$

With the above definitions it is guaranteed that $R_{SW,PM}$, $R_{ST,PM}$ and $R_{PM,A}$ are always positive. The general form of (11) is chosen to model the laminar as well as turbulent air flow inside the air gap and around the rotor shaft surface, respectively. The formulation (11) is designed with a minimum number of coefficients (only three per resistance) to limit the total number of unknown parameters within the identification process. To limit the search room the maximum values $a_{i,j,max}$, $b_{i,j,max}$ and $R_{i,j,0,max}$ are conservatively estimated based on the analytical formulations in [37], [54] in advance.

C. State-Space Representation

Based on the above model description a compact mathematical expression describing the LPTN system behaviour can be given in the state-space form:

$$\begin{aligned} \dot{\boldsymbol{x}} &= \boldsymbol{A}(n)\boldsymbol{x} + \boldsymbol{B}(\boldsymbol{\vartheta}, n, I)\boldsymbol{u}(n, I) \\ \boldsymbol{y} &= \boldsymbol{C}\boldsymbol{x} + \boldsymbol{D}\boldsymbol{u} \end{aligned} \tag{12}$$

where

$$\begin{aligned} \boldsymbol{x} &= \boldsymbol{\vartheta} = [\vartheta_{SY} \quad \vartheta_{SW} \quad \vartheta_{ST} \quad \vartheta_{PM}] \\ \boldsymbol{u} &= \left[\widetilde{P}_{v,Cu} \quad \widetilde{P}_{v,res} \quad \vartheta_C \quad \vartheta_A\right] \\ \boldsymbol{A} &= \mathbb{R}^{4\times4}, \quad \boldsymbol{B} = \mathbb{R}^{4\times4}, \quad \boldsymbol{C} = \boldsymbol{I}^{4\times4}, \quad \boldsymbol{D} = 0 \end{aligned} \tag{13}$$

Here, bold symbols denote vectorial or matrix quantities. $\boldsymbol{C} = \boldsymbol{I}$ is the identity matrix since the investigated motor is equipped with several thermal sensors in all considered motor parts. It should be noted that (12) is a linear parameter-varying (LPV) model as $\boldsymbol{A}$ and $\boldsymbol{B}$ are depending on so-called scheduling variables, which are the speed n, the stator current I and the internal states $\boldsymbol{\vartheta}$.

D. Discretisation of State-Space Models

For identification and validation purpose, the LPTN state space model (12) has to be discretised. Assuming, the input quantities $\boldsymbol{u}$ are constant during a sampling instant $t_k = kT_s$, the transition matrix of (12) can be calculated

$$\boldsymbol{\Phi} = e^{\boldsymbol{A}T_s} \tag{14}$$

where T_s denotes the sampling time. Then, the discrete-time input matrix is given by

$$\boldsymbol{H} = \int_0^{T_s} e^{\boldsymbol{A}T_s} \mathrm{d}\tau_s \boldsymbol{B} \tag{15}$$

Since the system matrix $\boldsymbol{A}$ and the input matrix $\boldsymbol{B}$ are varying during operation, $\boldsymbol{\Phi}$ and $\boldsymbol{H}$ have to be re-calculated every time the scheduling-variables change. As the evaluation of the

transition and discrete-time input matrix is rather computational demanding, the advantage of a small LPTN with only a few nodes and parameters is counteracted from the computational resource point of view. Hence, the explicit Euler method was applied instead of the exact discretisation. Here, $\boldsymbol{\Phi}$ and $\boldsymbol{H}$ are replaced by their first-order approximations:

$$\begin{aligned} \tilde{\boldsymbol{\Phi}} &= \boldsymbol{I} + T_s \boldsymbol{A} \\ \tilde{\boldsymbol{H}} &= T_s \boldsymbol{B} \end{aligned} \tag{16}$$

with $\boldsymbol{I}$ as identity matrix. The resulting discrete-time model is then given by:

$$\frac{1}{T_s}\left(\boldsymbol{\vartheta}[k+1] - \boldsymbol{\vartheta}[k]\right) = \boldsymbol{A}[k]\boldsymbol{\vartheta}[k] + \boldsymbol{B}[k]\boldsymbol{\vartheta}[k] \tag{17}$$

It should be kept in mind, that the reduction of computational efforts comes at a limited numerical stability for Euler-discretised systems. As shown in [55] the eigenvalues s_i of the continuous-time system have to satisfy

$$\left| s_i + \frac{1}{T_s} \right| < \frac{1}{T_s} \tag{18}$$

to guarantee numerical stability. Besides the general numerical stability, the sampling time T_s should be chosen as a trade-off between computational load and numerical accuracy. For this contribution $T_s = 1\ \mathrm{s}$ was applied.

IV. Parameter Identification

The identification objective is to identify the parameters of (17) in order to decrease the output error:

$$\boldsymbol{e} = \boldsymbol{\vartheta} - \hat{\boldsymbol{\vartheta}} \tag{19}$$

Hence, a suitable cost function J is required. This cost function should lead to a robust and accurate model i.e. the stationary and transient deviations should be small and the statistical variance of the output error should have white-noise form. In this context, robustness means that the accuracy is not only satisfying when the identified model is excited with the already known training data, but also when new validation data is applied (cross-validation). Against this background, the maximum-likelihood cost function is a suitable and well-known approach [56]:

$$J(\boldsymbol{p}) = \pi_{\boldsymbol{\vartheta}}(\hat{\boldsymbol{\vartheta}}|\boldsymbol{p}) \tag{20}$$

Here, π the probability density for fixed data $\boldsymbol{\vartheta}$ compared to the model outputs $\hat{\boldsymbol{\vartheta}}$ and $\boldsymbol{p}$ is the parameter vector which have to be manipulated to maximise (20). Here, $\boldsymbol{p}$ contains all unknown parameters defined in the general framework from Section III-A and III-B. For multiple-input and multiple-output state-space models (20) can be rewritten:

$$J(\boldsymbol{p}) = \det\left(\sum_{k=1}^{N} \boldsymbol{e}(k,\boldsymbol{p})\boldsymbol{e}(k,\boldsymbol{p})^T\right) \tag{21}$$

Above k is the sampling index and (21) can be interpreted as a modified output error covariance matrix, as well. Finally, the parameter identification can be interpreted as constrained optimisation task

$$\hat{\boldsymbol{p}} = \arg\min_{\boldsymbol{p}} J(\boldsymbol{e}) \quad \text{s.t. } \boldsymbol{g}(\boldsymbol{p}) \leq 0,\ \boldsymbol{h}(\boldsymbol{p}) = 0 \tag{22}$$

with $\boldsymbol{g}$ and $\boldsymbol{h}$ as general boundary conditions. Proper definitions of $\boldsymbol{g}$ help to reduce the search room in the parameter plane increasing the probability to identify suitable parameter values. The most important constraints are defined in the general framework from Section III-A and III-B. Here, well-known analytical formulations from the white-box LPTN approaches (e.g. [23], [25]) can be used to pre-calculated most of the considered parameters. With these rough estimates lower and upper bounds for the optimisation process can be chosen by the user. The analytically calculated parameter estimates for the investigated PMSM of this contribution are shown in [28].

A. Particle Swarm Optimisation

As the output error $\boldsymbol{e}$ is non-linear-dependent on the parameters $\boldsymbol{p}$ in the $\boldsymbol{A}$ and $\boldsymbol{B}$ matrices for state-space models, (22) is a non-linear, non-convex and multidimensional optimisation problem [56]. Also, the LPTN parameters from Section III are linear and non-linear depending on the scheduling parameters. Using standard gradient-based optimisation algorithms involve the risk to converge into local optima depending on the initialisation. Simple 'multi-start' approaches aren't feasible, since the amount of optimisation variables is too high. In total, 30 parameters have to be identified (see Tab. I), but based on the framework in Section III and the knowledge from [28], the search interval for every parameter can be limited to a manageable extent. To find the global optimum of (22), a particle swarm algorithm (PSO) was combined with sequential quadratic programming (SQP). A Simulink model of (17) has been set up and the unknown parameter values are the optimisation variables of the PSO and the SQP. Here, the optimisation process can be massively parallelised which is a major advantage of the proposed method.

The PSO is a meta-heuristic optimisation tool and was proposed first by Kennedy and Eberhart in 1995 [57]. The optimisation idea is based on the cooperation of multiple particles in one or several swarms which are exploring the search room. Each particle consists of its actual position $\boldsymbol{x}_i$, its actual velocity $\boldsymbol{v}_i$ and its historic best position $\boldsymbol{p}_i$. Since one particle would have no chance to detect the global optimum in complex optimisation problems the particles inform each other in defined neighbourhoods. To ensure a good balance between exploration and local optimisation, influences from randomness as well as active swarm control methods have to be taken into account. More general information regarding the PSO method can be found in [58]. For the given parameter identification task one swarm with a random neighbourhood structure and 300 particles had been set up. The particle positions (i.e. the search room) and the particle velocities had been limited based on the a-priori system knowledge from Section III. Also, the so-called 'inertia weight'-method had been used to allow a comprehensive exploration of the entire search room at the beginning following a more local search at the end of the PSO iterations [58]. First, possible parameter sets $\hat{\boldsymbol{p}}$ had been identified by the PSO and in a second step a reduced number of possible candidates $\hat{\boldsymbol{p}}$ had been given to a standard SQP-algorithm for a very accurate local optimisation. Then, the overall best parameter set $\hat{\boldsymbol{p}}$ had been chosen for validation purpose. It should be noted, that the proposed approach is non-deterministic and thus one cannot evaluate, if the the real global optimum was found. Therefore, the independent cross-validation is important to evaluate the resulting model performance.

Test bench measurements with a duration of roughly $40\ \mathrm{h}$ had been used as training data. Here, general considerations (e.g. optimal sampling time, optimal experiment duration,...) on how to design empirical experiments for parameter identification task have been taken into account from the well-known literature (see [56], [59]). The system inputs as well as the scheduling variables from (13) have been persistently excited in the complete possible operation range of the investigated motor. The obtained training data is then applied to (22) to retrieve the LPTN model parameters in a global LPV approach manner ('one shot' to identify all parameters). The identified parameter values are given in Tab. I.

V. Cross-Validation

Cross-validation implies that the input data strictly differ from that used during the training phase. The model inputs in Fig. 5 and Fig. 7 have been compared to the training data in terms of cross-correlation analysis to ensure a true cross-validation scenario. In Fig. 5 a load profile based on the US Federal-Test-Procedure-75 driving cycle for a electric subcompact vehicle

TABLE I. IDENTIFIED PARAMETER VALUES

Parameter	Identified Value	Parameter	Identified Value
C_{SY}	$5.59 \cdot 10^3$ J/K	C_{SW}	$2.62 \cdot 10^3$ J/K
C_{ST}	$2.91 \cdot 10^3$ J/K	C_{PM}	$1.08 \cdot 10^4$ J/K
$R_{SY,SW}$	0.289 K/W	$R_{SY,ST}$	0.013 K/W
$R_{SW,ST}$	0.019 K/W	$R_{C,SY,0}$	0.017 K/W
$\alpha_{C,SY}$	-0.66 %/K	$R_{ST,PM,0}$	0.599 K/W
$a_{ST,PM}$	0.093 K/W	$b_{ST,PM}$	0.781
$R_{SW,PM,0}$	1.149 K/W	$a_{SW,PM}$	0.361 K/W
$b_{SW,PM}$	1.013	$R_{PM,A,0}$	2.451 K/W
$a_{PM,A}$	0.148 K/W	$b_{PM,A}$	0.137
$R_{s,0}$	14.1 mΩ	$\beta_{Cu,1}$	0.315
$\beta_{Cu,2}$	0.616	α_{Fe}	-0.71 %/K
$k_{1,0}$	0.719	$k_{1,1}$	-0.059 1/A
$k_{1,2}$	0.069 min	$k_{1,3}$	-0.619 min/A
$k_{2,0}$	0.742	$k_{2,1}$	-0.213 1/A
$k_{2,2}$	-0.023 min	$k_{2,3}$	-0.474 min/A

is shown. For simplification reasons the ambient and cooling temperature are kept constant. It is obvious that the estimated temperatures are close to the measured ones and the maximum temperature deviation for all four nodes is in the range of $5\ ^\circ$C. Moreover, the bias

$$\text{Bias}_i = \frac{1}{N}\sum_{k=1}^{N} e_i(k, \boldsymbol{p}) \tag{23}$$

and the best-fit value

$$\text{BF}_i = \left(1 - \frac{|\boldsymbol{e}_i(k, \boldsymbol{p})|}{|\boldsymbol{\vartheta}_i - \overline{\boldsymbol{\vartheta}}_i|}\right) \cdot 100\ \% \tag{24}$$

prove a satisfying identification result [59]. In addition, the histograms of the corresponding estimation errors are shown in Fig. 6. Here, the stator yoke as well as teeth error distributions are very close to ideal white-noise form and the stator winding distribution is of biased white-noise form. Referring to [56], [59] white-noised estimation error distributions are a strong evidence of a robust and accurate identification result. However, the error distribution of the permanent magnet temperature in Fig. 6 is not a typical white-noise distribution giving rise to further thermal model improvements.

In Fig. 7 another load profile with a more significant thermal excitation is shown. Here, the cooling temperature is varying and also the ambient air temperature is changing slightly. It is obvious that these exogenous temperature profiles are unrealistic from the viewpoint of industry applications (e.g. automotive driving cycles). This circumstance is caused by limited capabilities to change the ambient air and cooling liquid temperature at the test bench during an experiment. Therefore, the applied exogenous temperature profiles give only a preliminary evidence regarding the correct modelling of external heat paths in the proposed model. Nevertheless, it should be noted that most publications in this field facing the same problem and therefore lacking information about how their models behave under realistic exogenous temperature profiles during validation experiments.

In Fig. 7 the maximum stator temperature deviations are again in the range of $5\ ^\circ$C, the maximum PM deviation is slightly larger with approximately $8\ ^\circ$C. The bias and BF values are again in a suitable range. Also, the estimation error histograms are given in Fig. 8. Again, the three stator estimation error distributions are close to the ideal white-noise form, but the permanent magnet temperature errors are related to a normalised distribution. Therefore, the estimation result regarding the permanent magnets can be improved in future investigations.

A. Further Discussion of Model Performance

As stated before, the temperature estimation accuracy regarding the considered stator components seems to be satisfying in the complete operation range. In contrast, the permanent magnet temperature estimation should be subject to further improvement. One possible way is to extend the LPTN structure in Fig. 2 by adding more nodes to the rotor part. In the current LPTN configuration in Fig. 2, the resistance $R_{PM,A}$ is very abstract as the rotor shaft is not only thermally connected to the surrounding ambient air at the test bench, but also to the end-cap air inside the motor housing, to the bearings, and to the load machine through a mechanical coupling device. A separate modelling of these parts can increase the estimation accuracy, but comes at the cost of increasing computational efforts to execute the resulting model in real-time. Also, the trade-off between model flexibility and robustness (bias-variance-dilemma, [59]) should be taken into account since an increased node and parameter amount can lead to identifications problems.

Another opportunity to increase the PM estimation accuracy is to extend the general definitions regarding $R_{PM,A}$. In Section III-B it is defined in the same way as the air-gap resistances, which may unsuitable for this heat path. Therefore, other equation types of $R_{PM,A}$ can be investigated in the future. Also, the proposed identification process can be modified. A stronger weighting of the PM temperature in contrast to the other motor temperature in the cost function (21) can lead to improved PM estimation accuracy, which may comes at the cost of decreased stator temperature estimation accuracy. In addition, other types of cost functions or different optimisation methods can be investigated.

Notwithstanding the above, the correct modelling of the heat path from rotor shaft to the external motor surrounding is a challenging task in many industrial applications. Other devices in close connection to the motor can introduce additional heat flows which may have an significant impact on the overall thermal motor behaviour (e.g. engine bays of hybrid electric vehicles with numerous auxiliaries). Hence, a suitable definition of (sub-)system boundaries regarding the thermal modelling of electric motors in complex thermal environments is a key issue.

VI. CONCLUSION

The key achievements of this contribution are:

- Proving general feasibility of global LPV-identification for thermal motor models (first time in literature)
- Providing a design and identification method for LPTN with incomplete motor information
- Realising an estimation error of $8\ ^\circ$C for the most important motor parts under complex load profiles with a low-order LPTN

A computationally efficient 4-node LPTN considering the stator yoke, stator teeth, stator winding and permanent magnet of a automotive traction PMSM has been designed. A-priori system knowledge about the constant and varying parameters has been used to limit the amount of unknown parameters and the resulting search room, respectively. A loss model based on measured motor losses is utilised and the exact loss distribution regarding the considered motor components is interpreted as a part of the parameter identification. Consequently, potentially less accurate FEA loss calculations can be avoided. The global LPV-LPTN identification is realised with the help of particle swarm optimisation in combination with sequential quadratic programming to prevent converging in suboptimal local minima. The parametrised thermal model shows suitable accuracy based on two different cross-validation load profiles. The achieved maximum output errors in the stator are convincing and the error bias values are close to zero. Evaluating the estimation error distributions potential for improvement regarding the permanent magnet temperature is identified since the desired white-noise form was not achieved. Consequently, future investigations should focus on the permanent magnet node improving the estimation accuracy utilising better identification methods or

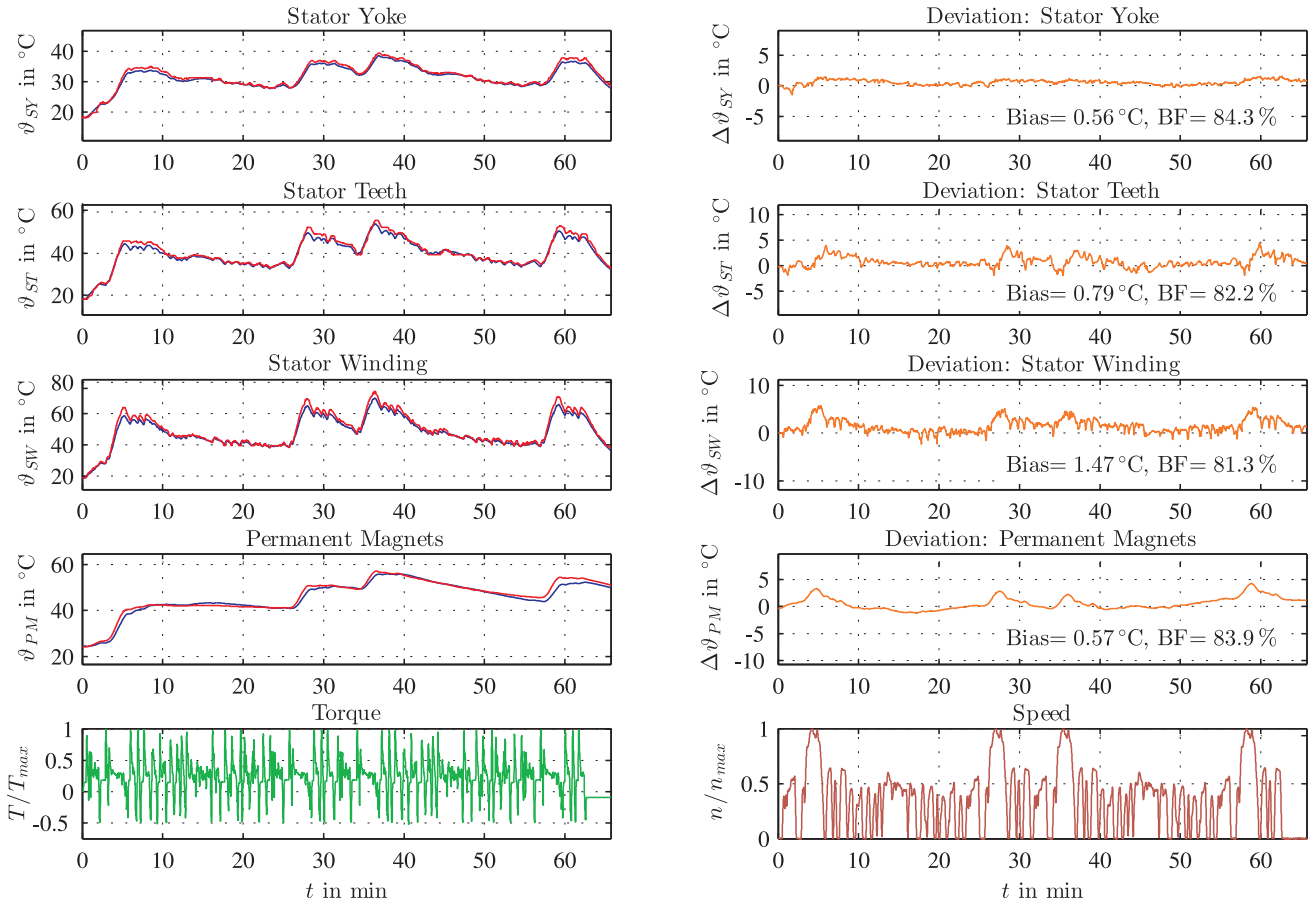

Fig. 5. Cross-validation based on Federal-Test-Procedure-75 driving cycle (red lines = measured temp., blue lines = estimated temp., $\vartheta_C = \vartheta_A = 20\,°\mathrm{C}$)

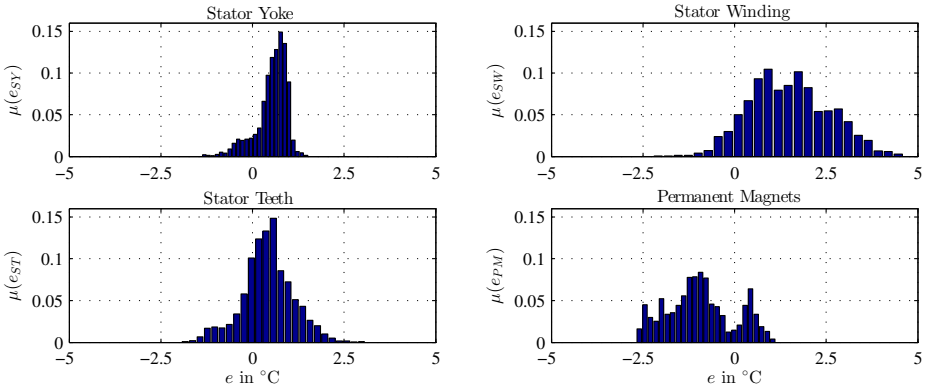

Fig. 6. Histograms of estimation errors regarding cross-validation based on Federal-Test-Procedure-75 driving cycle (see Fig. 5)

more degree of freedoms regarding the thermal model structure. Also, cross-validation scenarios with realistic cooling liquid and ambient air temperature profiles for automotive driving cycles should be considered in the future.

References

[1] R. Rothe and K. Hameyer, "Life Expectancy Calculation for Electric Vehicle Traction Motors Regarding Dynamic Temperature and Driving Cycles," in *IEEE International Electric Machines & Drives Conference (IEMDC)*, 2011.

[2] D. Huger and D. Gerling, "An Advanced Lifetime Prediction Method for Permanent Magnet Synchronous Machines," in *Interntional Conference on Electriclal Machines (ICEM)*, 2014.

[3] J. Lemmens, P. Vanassche, and J. Driesen, "Optimal Control of Traction Motor Drives Under Electrothermal Constraints," *IEEE Journal of Emerging and Selected Topics in Power Electronics*, vol. 2, no. 2, pp. 249–263, 2014.

[4] S. von Malottki, M. Gregor, A. Wanke, and K. Hameyer, "Magnet Design Based on Transient Behavior of an IPMSM in Event of Malfunction," in *Interntional Conference on Electriclal Machines (ICEM)*, 2014.

[5] L. Chen, D. Hopkinson, J. Wang, A. Cockburn, M. Sparkes, and W. O'Neill, "Reduced Dysprosium Permanent Magnets and Their Applications in Electric Vehicle Traction Motors," *IEEE Transactions on Magnetics*, 2015.

[6] T. Sebastian, "Temperature Effects on Torque Production and Efficiency of PM Motors Using NdFeB Magnets," *IEEE Transactions on Industry Applications*, vol. 31, no. 2, pp. 353–357, 1995.

[7] O. Wallscheid and J. Böcker, "Wirkungsgradoptimale Arbeitspunktsteuerung für einen permanenterregten Synchronmotor mit vergrabenen Magneten unter Berücksichtigung von Temperatureinflüssen (in German)," in *International ETG-Congress*, 2013.

[8] M. Ganchev, B. Kubicek, and H. Kappeler, "Rotor Temperature Monitoring System," in *International Conference on Electrical Machines*, 2010.

[9] C. Mejuto, M. Mueller, M. Shanel, A. Mebarki, M. Reekie, and D. Staton, "Improved Synchronous Machine Thermal Modelling," in *International Conference on Electrical Machines (ICEM)*, 2008.

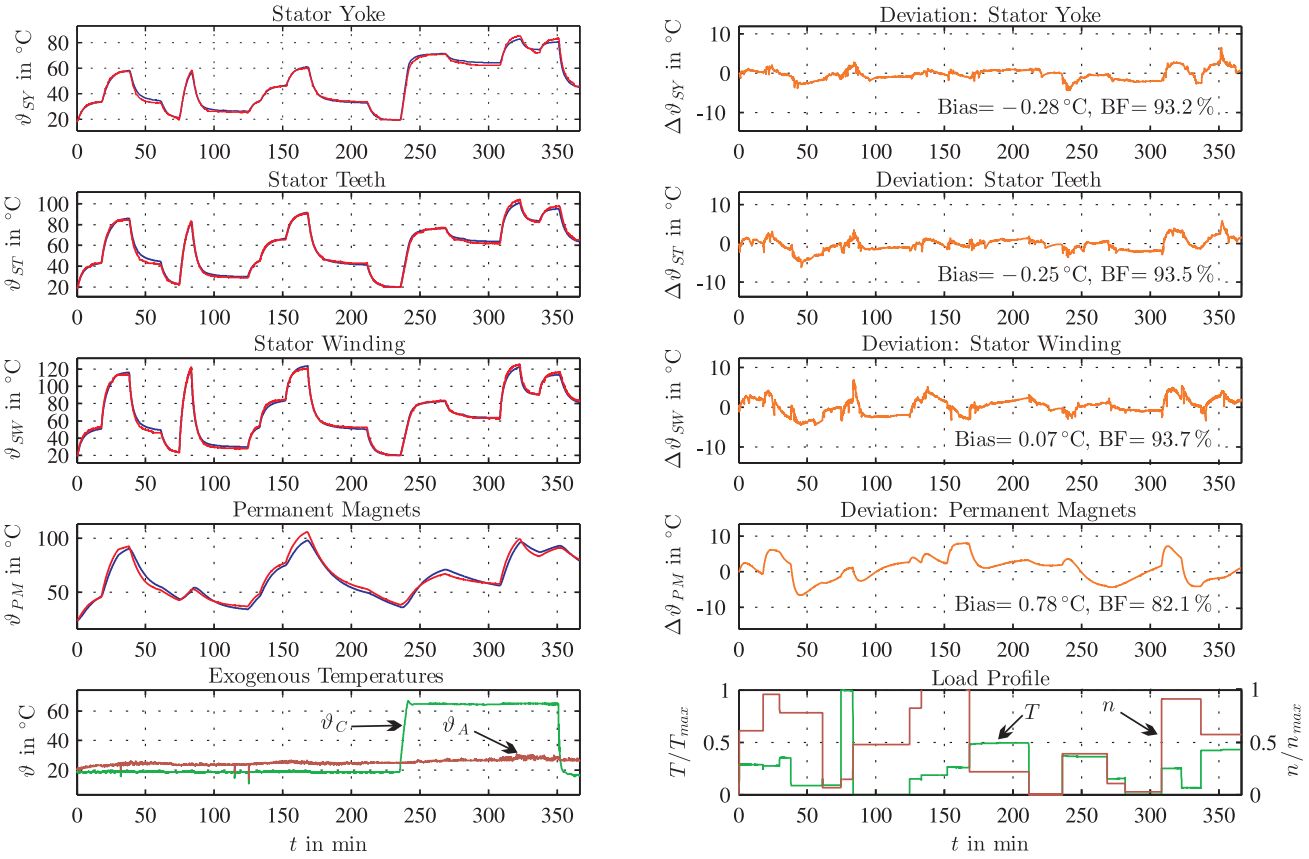

Fig. 7. Cross-validation based on artificial heavy-duty load profile (red lines = measured temp., blue lines = estimated temp.)

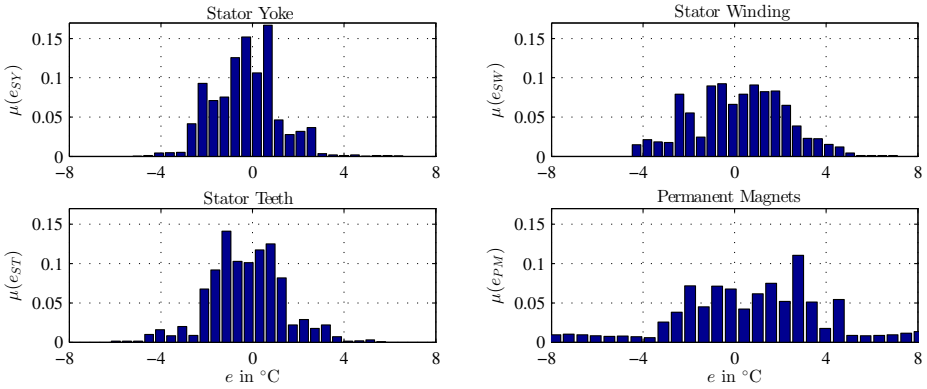

Fig. 8. Histogram of estimation errors regarding cross-validation based on artificial heavy-duty load profile (see Fig. 7)

[10] S. Stipetic, M. Kovacic, Z. Hanic, and M. Vrazic, "Measurement of Excitation Winding Temperature on Synchronous Generator in Rotation Using Infrared Thermography," *IEEE Transactions on Industrial Electronics*, vol. 59, no. 5, pp. 2288–2298, 2012.

[11] A. Specht, O. Wallscheid, and J. Böcker, "Determination of Rotor Temperature for an Interior Permanent Magnet Synchronous Machine Using a Precise Flux Observer," in *International Power Electronics Conference (IPEC)*, 2014.

[12] D. D. Reigosa, F. Briz, P. Garcia, J. M. Guerrero, and M. W. Degner, "Magnet Temperature Estimation in Surface PM Machines Using High-Frequency Signal Injection," *IEEE Transactions on Industry Applications*, vol. 45, no. 4, pp. 1468–1475, 2010.

[13] M. Ganchev, C. Kral, H. Oberguggenberger, and T. Wolbank, "Sensorless Rotor Temperature Estimation of Permanent Magnet Synchronous Motor," in *Annual Conference on IEEE Industrial Electronics Society*, 2011.

[14] S. D. Wilson, P. Stewart, and B. P. Taylor, "Methods of Resistance Estimation in Permanent Magnet Synchronous Motors for Real-Time Thermal Management," *IEEE Transactions on Energy Conversion*, vol. 10, no. 3, pp. 698–707, 2010.

[15] O. Wallscheid, T. Huber, W. Peters, and J. Böcker, "Real-Time Capable Methods to Determine the Magnet Temperature of Permanent Magnet Synchronous Motors - A Review," in *Annual Conference of the IEEE Industrial Electronics Society*, 2014.

[16] G. D. Demetriades, H. Z. D. L. Parra, E. Andersson, and H. Olsson, "A Real-Time Thermal Model of a Permanent-Magnet Synchronous Motor," *IEEE Transactions on Power Electronics*, vol. 25, no. 2, pp. 463–474, 2010.

[17] T. Huber, W. Peters, and J. Böcker, "A Low-Order Thermal Model for Monitoring Critical Temperatures in Permanent Magnet Synchronous Motors," in *International Conference on Power Electronics, Machines and Drives (PEMD)*, 2014.

[18] A. Boglietti, A. Cavagnino, D. Staton, M. Shanel, M. Mueller, and C. Mejuto, "Evolution and Modern Approaches for Thermal Analysis of Electrical Machines," *IEEE Transactions on Industrial Electronics*, vol. 56, iss. 3, pp. 871–882, 2009.

[19] T. Huber, W. Peters, and J. Böcker, "Monitoring Critical Temperatures in Permanent Magnet Synchronous Motors Using Low-Order Thermal Models," in *International Power Electronics Conference (IPEC)*, 2014.

[20] C. Kral, A. Haumer, and S. B. Lee, "A Practical Thermal Model for the Estimation of Permanent Magnet and Stator Winding Temperatures," *IEEE Transactions on Power Electronics*, vol. 29, no. 1, pp. 455–464, 2014.

[21] A. Boglietti, E. Carpaneto, M. Cossale, A. L. Borlera, D. Staton,

and M. Popescu, "Electrical Machine First Order Short-Time Thermal Transients Model: Measurements and Parameter Evaluation," in *Annual Conference of the IEEE Industrial Electronics Society (IECON)*, 2014.

[22] F. Boseniuk and B. Ponick, "Parameterization of Transient Thermal Models for Permanent Magnet Synchronous Machines Exclusively Based on Measurements," in *International Symposium on Power Electronics, Electrical Drives, Automation and Motion*, 2014.

[23] A. Boglietti, A. Cavagnino, M. Lazzari, and M. Pastorelli, "A Simplified Thermal Model for Variable-Speed Self-Cooled Industrial Induction Motor," *IEEE Transactions on Industry Applications*, vol. 39, no. 4, pp. 945–952, 2003.

[24] J. Fan, C. Zhang, Z. Wang, Y. Dong, C. E. Nino, A. R. Tariq, and E. G. Strangas, "Thermal Analysis of Permanent Magnet Motor for the Electric Vehicle Application Considering Driving Duty Cycle," *IEEE Transactions on Magnetics*, vol. 46, iss. 6, pp. 2493–2496, 2010.

[25] P. Mellor, D. Roberts, and D. Turner, "Lumped Parameter Thermal Model for Electrical Machines of TEFC Design," *IEE Proceedings B Electric Power Applications*, vol. 138, iss. 5, pp. 205–218, 1991.

[26] D. Roberts, "The Application of an Induction Motor Thermal Model to Motor Protection and other Functions," Ph.D. dissertation, University Liverpool, 1986.

[27] J. Nerg, M. Rilla, and J. Pyrhönen, "Thermal Analysis of Radial-Flux Electrical Machines With a High Power Density," *IEEE Transactions on Industrial Electronics*, vol. 55, no. 10, pp. 3543–3554, 2008.

[28] O. Wallscheid and J. Böcker, "Design and Identification of a Lumped-Parameter Thermal Network for Permanent Magnet Synchronous Motors Based on Heat Transfer Theory and Particle Swarm Optimisation," in *European Conference on Power Electronics and Applications*, 2015.

[29] L. Idoughi, X. Mininger, F. Bouillault, L. Bernard, and E. Hoang, "Thermal Model With Winding Homogenization and FIT Discretization for Stator Slot," *IEEE Transactions on Magnetics*, vol. 47, no. 12, pp. 4822–4826, 2011.

[30] S. Nategh, O. Wallmark, M. Leksell, and S. Zhao, "Thermal Analysis of a PMaSRM Using Partial FEA and Lumped Parameter Modeling," *IEEE Transactions on Energy Conversion*, vol. 27, no. 2, pp. 477–488, 2012.

[31] S. Nategh, Z. Huang, A. Krings, O. Wallmark, and M. Leksel, "Thermal Modeling of Directly Cooled Electric Machines Using Lumped Parameter and Limited CFD Analysis," *IEEE Transactions on Energy Conversion*, vol. 28, no. 4, pp. 979–990, 2013.

[32] D. Kuehbacher, A. Kelleter, and D. Gerling, "An Improved Approach for Transient Thermal Modeling using Lumped Parameter Networks," in *IEEE International Electric Machines & Drives Conference (IEMDC)*, 2013.

[33] F. Qi, A. Stippich, M. Guettler, M. Neubert, and R. W. D. Doncker, "Methodical Considerations for Setting Up Space-Resolved Lumped-Parameter Thermal Models for Electrical Machines," in *International Conference on Electrical Machines and Systems (ICEMS)*, 2014.

[34] W. H. Tang, S. He, E. Prempain, Q. H. Wu, and J. Fitch, "A Particle Swarm Optimiser with Passive Congregation Approach To Thermal Modelling For Power Transformers," in *IEEE Congress on Evolutionary Computation*, 2005.

[35] F. Qi., M. Schenk, and R. D. Doncker, "Discussing Details of Lumped Parameter Thermal Modeling in Electrical Machines," in *International Conference on Power Electronics, Machines and Drives (PEMD)*, 2014.

[36] R. Wrobel, J. Goss, A. Mlot, and P. H. Mellor, "Design Considerations of a Brushless Open-Slot Radial-Flux PM Hub Motor," *IEEE Transactions on Industry Applications*, vol. 50, no. 3, pp. 1757–1767, 2014.

[37] D. A. Howey, P. R. N. Childs, and A. S. Holmes, "Air-Gap Convection in Rotating Electrical Machines," *IEEE Transactions on Industrial Electronics*, vol. 59, no. 3, pp. 1367–1375, 2012.

[38] O. Sename, P. Gaspar, and J. Bokor, Eds., *Robust Control and Linear Parameter Varying Approaches - Application to Vehicle Dynamics*. Springer-Verlag Berlin Heidelberg, 2013.

[39] R. Toth, "Modeling and Identification of Linear Parameter-Varying Systems," Ph.D. dissertation, University Delft, 2008.

[40] F. Casella and M. Lovera, "LPV/LFT Modelling and Identification: Overview, Synergies and a Case Study," in *IEEE Multi-Conferencce on Systems and Control*, 2008.

[41] J. D. Caigny, J. F. Camino, and J. Swevers, "Interpolation-Based Modeling of MIMO LPV Systems," *IEEE Transactions on Control Systems Technology*, vol. 19, no. 1, pp. 46–63, 2011.

[42] Y. Bolea, A. Grau, and N. Chefdor, "MIMO LPV State-Space Identification of an Open-Flow Irrigation Canal for Control," in *IEEE International Conference on Industrial Informatics (INDIN)*, 2012.

[43] L. Lee and K. Poolla, "Identification of Linear Parameter-Varying Systems Using Nonlinear Programming," *Journal of Dynamic Systems, Measurement, and Control*, vol. 121, iss. 1, pp. 71–78, 1999.

[44] M. Nemani, R. Ravikanth, and B. A. Bamieh, "Identification of Linear Parametrically Varying Systems," in *Conference on Decision and Control*, 1995.

[45] W. H. Tang, Q. H. Wu, and Z. J. Richardson, "A Simplified Transformer Thermal Model Based on Thermal-Electric Analogy," *IEEE Transactions on Power Delivery*, vol. 19, no. 3, pp. 1112–1119, 2004.

[46] C. Schulte and J. Böcker, "Co-Simulation of an Electric Traction Drive," in *IEEE International Electric Machines & Drives Conference*, 2013.

[47] W. Peters, O. Wallscheid, and J. B?cker, "A Precise Open-Loop Torque Control for an Interior Permanent Magnet Synchronous Motor (IPMSM) Considering Iron Losses," in *Annual Conference of the IEEE Industrial Electronics Society (IECON)*, 2012.

[48] W. Peters and J. Böcker, "Discrete-Time Design of Adaptive Current Controller for Interior Permanent Magnet Synchronous Motors (IPMSM) with High Magnetic Saturation," in *Annual Conference of the IEEE Industrial Electronics Society (IECON)*, 2013.

[49] University of Paderborn - Department Power Electronics and Electrical Drives. (2015). [Online]. Available: http://wwwlea.uni-paderborn.de/en.html

[50] W. Peters, T. Huber, and J. Böcker, "Voltage Controller for Flux Weakening Operation of Interior Permanent Magnet Synchronous Motor in Automotive Traction Applications," in *IEEE International Electric Machines & Drives Conference (IEMDC)*, 2015.

[51] J. Schützhold and W. Hofmann, "Analysis of the Temperature Dependence of Losses in Electrical Machines," in *IEEE Energy Conversion Congress and Exposition (ECCE)*, 2013.

[52] A. Ladjimi and M. Mekideche, "Model for the Behavior of Magnetic Materials Hysteretis Taking Into Account the Temperature," in *International Multi-Conference on Systems, Signals and Devices*, 2009.

[53] N. Simpson, R. Wrobel, and P. H. Mellor, "Estimation of Equivalent Thermal Parameters of Impregnated Electrical Windings," *IEEE Transactions on Industry Applications*, vol. 49, no. 6, pp. 2505–2515, 2013.

[54] D. A. Staton and A. Cavagnino, "Convection Heat Transfer and Flow Calculations Suitable for Electric Machines Thermal Models," *IEEE Transactions on Industrial Electronics*, vol. 55, no. 10, pp. 3509–3516, 2008.

[55] J. Böcker, "Discrete-Time Model of an Induction Motor," *European Transactions on Electrical Power*, vol. 1, pp. 65–71, 1991.

[56] E. Walter and L. Pronzato, *Identification of Parametric Models*. Springer-Verlag Berlin Heidelberg, 1997.

[57] J. Kennedy and R. Eberhart, "Particle Swarm Optimization," in *IEEE International Conference on Neural Networks*, 1995.

[58] M. Clerc, *Particle Swarm Optimization*. ISTE, 2006.

[59] L. Ljung, *System Identifcation: Theory for the User*. Prentice Hall Inc., 1987.

Oliver Wallscheid received his bachelor and master degree (with honours) in industrial engineering from University of Paderborn, Germany, in 2010 and 2012, respectively. Since then, he has worked as a research associate for the Department of Power Electronics and Electrical Drives at the University of Paderborn pursuing his doctoral degree. His research focus is on the thermal modelling of highly utilised traction drives and the consideration of temperature effects in terms of control design.

Joachim Böcker is full professor and head of the department of Power Electronics and Electrical Drives at the University of Paderborn, Germany. He studied electrical engineering at Berlin University of Technology, Germany, where he received the Dipl.-Ing. and Dr.-Ing. degrees in 1982 and 1988, respectively. He was with AEG and Daimler research as head of the control engineering team of the electrical drive systems laboratory from 1988 to 2001. In 2001, he started his own business in the area of control engineering, electrical drives and power electronics. In 2003, he was appointed to the current professorship. The research areas of his group include electrical drives, particularly for EVs and HEVs, energy management strategies for vehicles and smart grids, and converters for power supplies, EV chargers, and renewables.